Neuron, Vol. 20, 995–1005, May, 1998, Copyright ©1998 by Cell Press

A Novel Inward Rectifier K^+ Channel with Unique Pore Properties

Grigory Krapivinsky, Igor Medina, Lily Eng, Luba Krapivinsky, Yinhai Yang, and David E. Clapham*
Howard Hughes Medical Institute
Children's Hospital Cardiovascular Division
and Harvard Medical School
Boston, Massachusetts 02115

Summary

We have cloned a novel K^+-selective, inward rectifier channel that is widely expressed in brain but is especially abundant in the Purkinje cell layer of the cerebellum and pyramidal cells of the hippocampus. It is also present in a wide array of tissues, including kidney and intestine. The channel is only 38% identical to its closest relative, Kir1.3 (Kir1-ATP–regulated inward rectifier K^+ [ROMK] family) and displays none of the functional properties unique to the ROMK class. Kir7.1 has several unique features, including a very low estimated single channel conductance (~50 fS), low sensitivity to block by external Ba^{2+} and Cs^+, and no dependence of its inward rectification properties on the internal blocking particle Mg^{2+}. The unusual pore properties of Kir7.1 seem to be explained by amino acids in the pore sequence that differ from corresponding conserved residues in all other Kir channel proteins. Replacement of one of these amino acids (Met-125) with the Arg absolutely conserved in all other Kir channels dramatically increases its single channel conductance and Ba^{2+} sensitivity. This channel would provide a steady background K^+ current to help set the membrane potential in cells in which it is expressed. We propose that the novel channel be assigned to a new Kir subfamily, Kir7.1.

Introduction

All cells spend most of their time with a negative voltage across their plasma membranes. A substantial fraction of an organism's energy is used in maintaining the unequal distribution of ions across the plasma membrane that set the stage for this to occur. However, it is the fact that K^+ channels are open more than other ion channels that creates the negative resting membrane potential. By holding cells close to the K^+ equilibrium potential, K^+ channels dominate the electrical behavior of cells. Not surprisingly, there are more types of K^+ channels than any other channel type, with the two major families (Kv, voltage-gated delayed rectifiers, and Kir, inward rectifiers) each having numerous subfamilies. Probably early in evolution, a two-transmembrane-spanning protein took part in forming the K^+-selective inward rectifier channel, which became the precursor of most ligand-independent ion channels. It is this class of channels that is open in its steady state to create the resting membrane potential that most cells obey.

*To whom correspondence should be addressed.

Kir channels are able to pass K^+ ions much more readily into the cell than out of it, despite the fact that inward K^+ current does not flow under physiologic conditions. One can speculate that the physiological significance of inward rectification is that internal blockers such as Mg^{2+} and polyamines may then regulate K^+ current. A more likely reason is that the simple ball valve design of Kir channels reduced the work cells needed to depolarize the membrane potential. By not having to overcome a large resting outward current, cells could be rapidly and efficiently depolarized, and between depolarizations only small amounts of K^+ ions were lost. For rapid repolarization, the larger conductance voltage-sensitive Kv channels were brought into play. Several Kir subfamilies (Kir1-ATP–regulated inward rectifier K^+ [ROMK], Kir3-G protein–gated inward rectifier K^+ [GIRK], and Kir6-ATP–sensitive K^+ channel [KATP]) are regulated by second messengers, largely to alter the bursting and pacing activity of cells like cardiac myocytes, neurons, and secretory cells. Other subfamilies, such as IRKs, seem to be responsible for reliably setting the resting membrane potential. In this paper, we describe a novel subfamily of Kirs, which is unique in all respects within the Kir class of channels.

All K^+ channel polypeptides share a homologous pore region believed to form an integral part of the K^+-selective pore (reviewed by Nichols and Lopatin, 1997). Representative channels of this class include the ATP-sensitive Kir1 (ROMK1; Ho et al., 1993), Kir2 (IRK1; Kubo et al., 1993a), the G protein–gated Kir3 channels (GIRK1; Kubo et al., 1993b), Kir4 and Kir5 (Bond et al., 1994), and Kir6 (IKATP when combined with the sulfanylurea receptor; Inagaki et al., 1995a). Unlike the six-transmembrane-spanning class of outwardly rectifying K^+ channels, Kir channels are weakly voltage dependent. Probably the most interesting feature of Kir channels is that their gating follows the Nernst potential as $[K^+]_o$ is changed (Hagiwara et al., 1976), indicating a K^+-binding site in the channel on its external surface (Ciani et al., 1978). The unitary conductance of Kir channels varies from 10–80 pS (Ho et al., 1993; Makhina et al., 1994; Inagaki et al., 1995a, 1995b; Krapivinsky et al., 1995; Aleksandrov et al., 1996). Although no specific blockers for Kir channels are known, they are all sensitive to extracellular Ba^{2+} and Cs^+ (Kubo et al., 1993a; Bond et al., 1994; Bredt et al., 1995; Takumi et al., 1995; Shuck et al., 1997).

Little is known about how ion channel pore structure selects for specific ions or how it relates to single channel conductance and kinetics. In seeking new members of the Kir family, we cloned and expressed a novel Kir channel subunit, which is remarkable for its uniquely low single channel conductance and low sensitivity to external Ba^{2+} blockade. These features appear to relate to unique amino acids in the pore region of the Kir7.1 channel. We hypothesize that the channel's main role is to reliably set the resting membrane potential. Its low conductance allows for significant precision in regulating membrane potential.

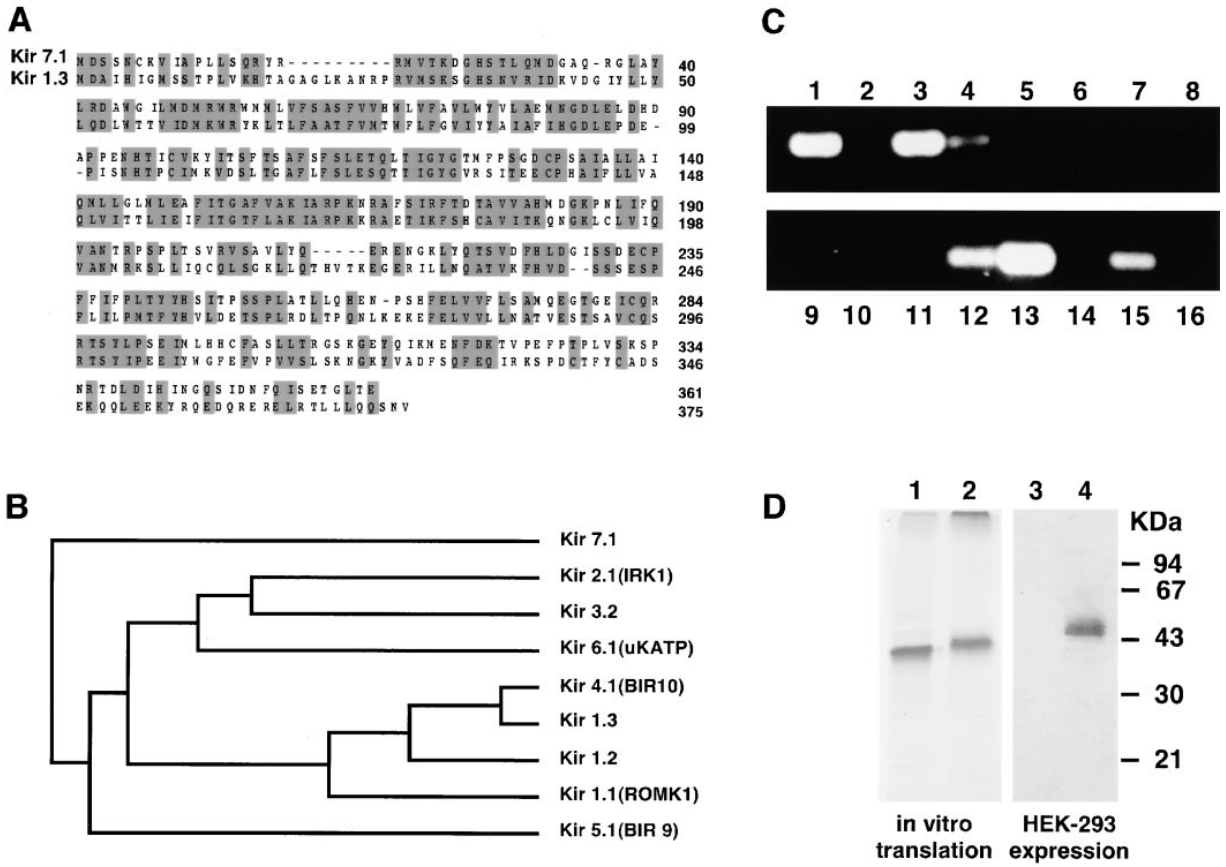

Figure 1. Primary Structure, Tissue Distribution, and Heterologous Expression of Kir7.1

(A) Comparison of Kir7.1 and Kir1.3 (ROMK subfamily) amino acid sequences (CLUSTAL alignment). Although Kir1.3 is the most closely related protein to Kir7.1, is is only 38% identical. Conserved and homologous amino acid residues are shaded.

(B) A dendrogram of the Kir channel family representatives illustrates dissimilarity between Kir7.1 and other family members. The dendrogram was generated using a progressive alignment method (GeneWorks, IntelliGenetics).

(C) Human multiple tissue cDNA panel PCR screening demonstrates expression of Kir7.1 in kidney, brain, and intestine and to a lesser extent in testis, liver, and prostate: (1) brain, (2) heart, (3) kidney, (4) liver, (5) lung, (6) pancreas, (7) placenta, (8) skeletal muscle, (9) colon, (10) ovary, (11) peripheral blood leucocyte, (12) prostate, (13) small intestine, (14) spleen, (15) testis, and (16) thymus.

(D, Left) In vitro translation of the Kir7.1 clone produced a single protein with an apparent MW of 37 kDa (lane 1). In vitro translation in the presence of canine microsomes yielded a slightly higher molecular weight (40 kDa) glycosylated protein (lane 2).

(D, Right) Anti-Kir7.2 antibody recognized a 45 kDa protein in HEK293 cells transfected with Kir7.2 cDNA (line 4) but not in vector-transfected cells (lane 3).

Results

A BLAST search of the GenBank Expressed Sequence Tag (EST) database using the Kir1.1 and Kir6.2 full-length coding sequences revealed a novel sequence from a human melanocyte library (clone *260707*). Translation of this clone yelded an amino acid sequence with homology in key regions of known inward rectifier K^+ channels but with significant differences from all known Kirs. Subsequent PCR analysis showed that a corresponding cDNA was present in a human brain cDNA library. We used the *260707* clone to screen a human fetal brain λ cDNA library (Uni-Zap XR, Stratagene). A single positive hybridizing phage was purified and the cDNA insert was sequenced. The 1276 bp insert contained a single open reading frame (ORF), which encoded a protein with 360 amino acids and had a predicted MW of 40.5 kDa. Hydrophobicity analysis was typical for Kir channel subunits with two transmembrane domains that flank the pore region containing the signature GYG motif (see Doyle et al., 1998).

The closest homolog to the cloned protein was human Kir1.3 (Shuck et al., 1997), a member of the ROMK subfamily of inward rectifier K^+ channels, with 38% identity at the amino acid level (Figure 1A). In contrast to other Kir1 (ROMK) subfamily members, the novel Kir sequence did not have a Walker type A motif (Walker et al., 1982) specifying sensitivity to ATP. Differences in the novel Kir sequence from the Kir1 family were significant enough that an alignment program placed it in a separate branch (Figure 1B). Although we have not yet identified other members of the subfamily, the low structural homology and the different biophysical properties of the channel have led us to propose that the channel be called Kir7.1, sequentially the newest member of the Kir family.

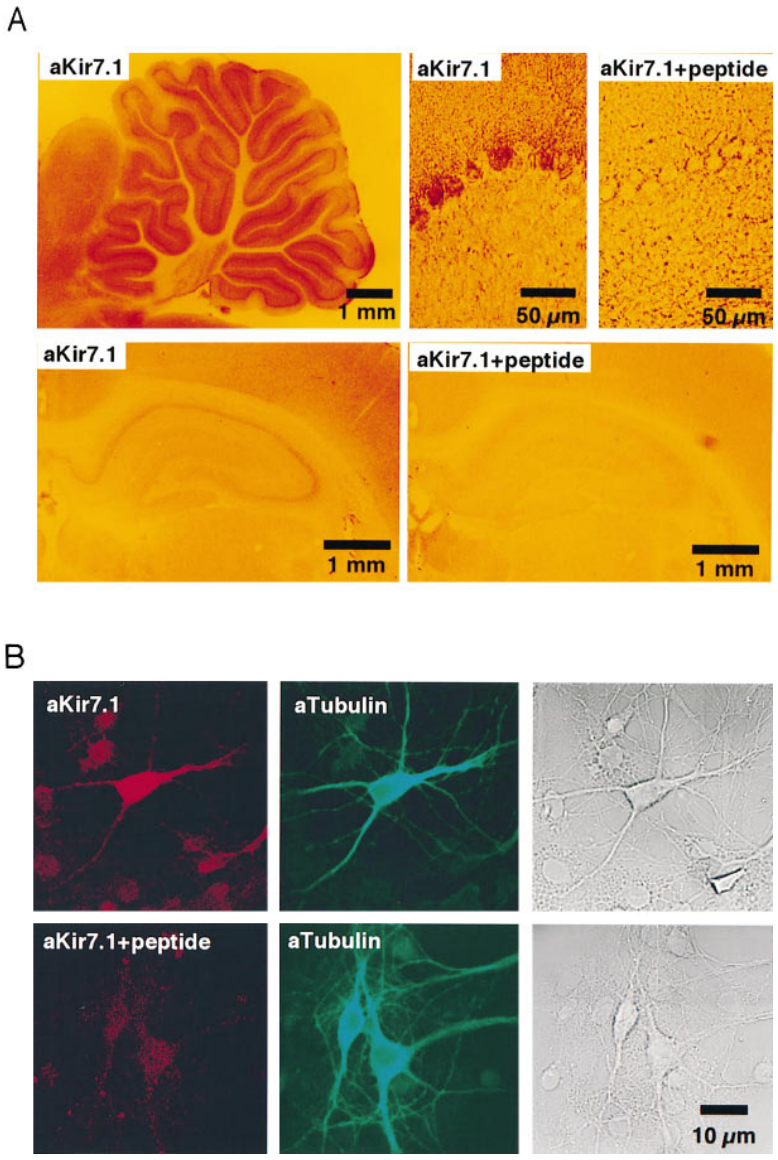

Figure 2. Immunolocalization of Kir7.1 in Rat Brain Slices and Primary Cultures of Hippocampal Cells

The specificity of immunolabeling was verified by immunostaining with the same aKir7.1 antibody preblocked with antigenic fusion protein.

(A, Top) Kir7.1 was expressed predominantly in the Purkinje cell layer of the cerebellum in rat brain slices. High magnification images show specifically labeled Purkinje cells.

(A, Bottom) Labeling of the pyramidal cell layer in hippocampus. Less intensive labeling is observed also in dentate gyrus, stratum oriens, and stratum radiatum.

(B) Kir7.1 is specifically expressed in neurons. The same cells are shown labeled by aKir7.1 (left), by anti-neurotubulin (middle), or simply via transmitted light. The lower panel shows cells labeled with aKir7.1 preblocked with antigen.

The EST *260707* clone initially used to probe the library contained 80% of the Kir7.1 ORF (including the pore region) and was identical to Kir7.1. PCR product sequences obtained from three independent human libraries (brain, kidney, small intestine; Clontech) also verified that the Kir7.1 sequence was correct and did not contain cloning artifacts. In vitro translation of the Kir7.1 clone produced a single protein with an apparent MW of 37 kDa. Translation in the presence of canine microsomes resulted in an increase in its apparent MW (Figure 1D), probably as a result of glycosylation and consistent with the glycosylation consensus sequence in Kir7.1's putative extracellular loop (Asn-95). Screening of human multiple tissue cDNA panels (MTC, Clontech) with primers specific for Kir7.1 demonstrated that the messenger RNA was most abundant in human brain, kidney, and small intestine. Less was present in testis, liver, and prostate (Figure 1C). Northern blots of tissue panels also confirmed Kir7.1 mRNA expression in brain and kidney (data not shown). Using Western blot analysis, we demonstrated that aKir7.1 antibody specifically recognized a 45 kDa protein in brain membrane preparations (data not shown). Kir7.1 immunoperoxidase staining of rat brain slices revealed diffuse labeling of all brain compartments when compared with negative controls. The Purkinje cell layer in the cerebellum and the pyramidal cell layer in the hippocampus (Figure 2A) were the two regions stained most intensively, suggesting that Kir7.1 was expressed specifically in neurons of brain tissue. Immunofluorescence staining of hippocampal cells in culture confirmed this point; anti-Kir7.1 antibody specifically labeled neurons but not glial cells (Figure 2B). The channel was evenly distributed in neuronal cell bodies and dendritic membrane. Simultaneous labeling of neurons with anti-GABA antibody demonstrated that Kir7.1 was expressed in both GABAergic and non-GABAergic neurons (data not shown).

To study the functional expression of the channel, the

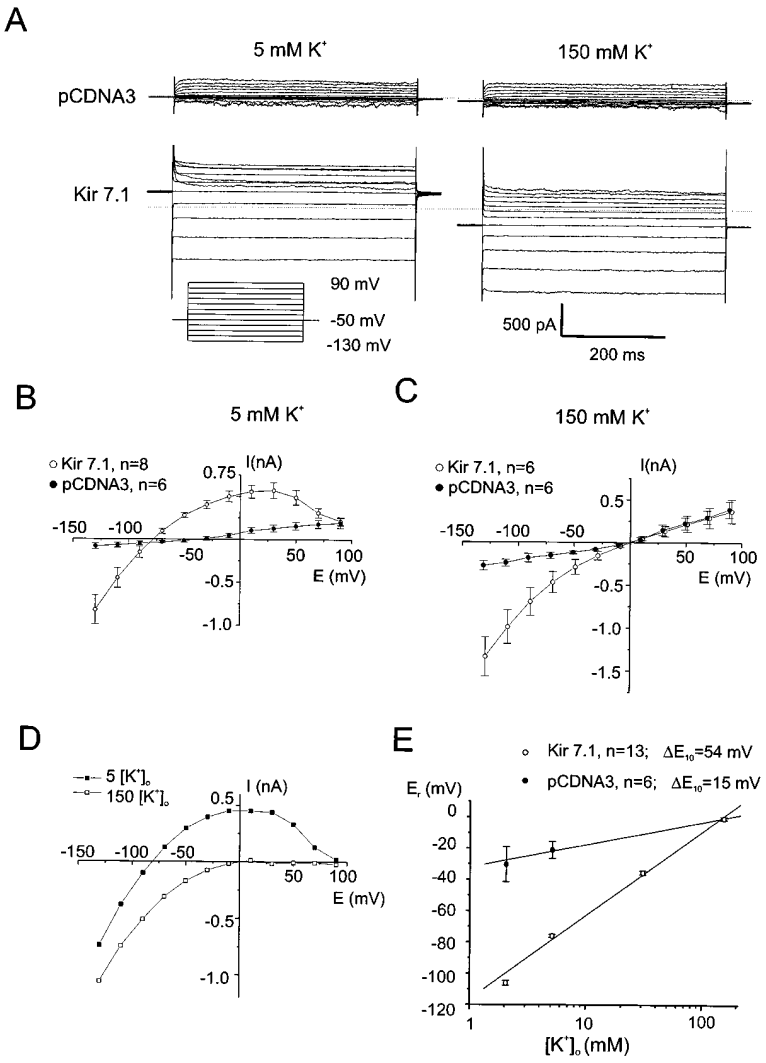

Figure 3. Electrophysiological Properties of Kir7.1 Expressed in Mammalian Cell Lines

(A) Currents measured in mock- and Kir7.1-transfected HEK293 cells. Currents were recorded in response to voltage-clamp steps from the holding potential (−50 mV) to voltages between −130 mV and +90 mV (ΔV = 20 mV) in 5 and 150 mM $[K^+]_o$. Horizontal dotted lines mark the zero current level.

(B and C) Mean I–V relations measured from cells expressing pcDNA 3.1 alone or Kir7.1 in the presence of 5 mM $[K^+]_o$ (B) or 150 mM $[K^+]_o$ (C). Current was plotted as the mean current measured isochronally between 400 and 450 ms of the 500 ms pulse.

(D) Net Kir7.1 current was obtained by subtraction of mock-transfected (pcDNA 3.1–transfected) from Kir7.1-transfected current in Figures 3B and 3C. Note that the I–V relation in 5 mM $[K^+]_o$ rectified weakly in comparison to the current measured in 150 mM $[K^+]_o$. Note that the slope of both curves increased with negative potentials.

(E) Reversal potentials measured from HEK cells transfected with Kir7.1 or pcDNA 3.1 plotted as a function of $[K^+]_o$ (±SEM, n = 13 and 6 as indicated). The data was fit by straight lines with slopes of 54 (Kir7.1) or 15 (pcDNA alone) mV/decade.

Similar Kir7.1 inward rectifier current was observed in all cells studied (n = 33 for HEK293, n = 21 for CHO-K1, and n = 8 for COS7 cells). Note that the I–V curve reached a plateau at potentials between 0 and 40 mV but that the slope became negative at more positive potentials. The slope of the E_r versus $[K^+]_o$ relation was −55 mV (n = 8) for CHO cells and −45 mV for COS7 cells (n = 5).

full-length Kir7.1 cDNA was subcloned into the pcDNA 3.1 vector and transfected into Green monkey kidney (COS7), human embryonic kidney (HEK293), and Chinese hamster ovary (CHO-K1) cells. An affinity-purified polyclonal antibody raised against the Kir7.1 C-terminal amino acid sequence recognized a 45 kDa protein in expressing but not in mock-transfected cells (Figure 1D). Whole-cell currents were measured from mock-transfected cells (transfected with the empty pcDNA 3.1 vector) and compared to cells transfected with Kir7.1 cDNA. Green fluorescent protein (GFP) was cotransfected into cells and GFP fluorescence used to select cells for recordings.

Figure 3 shows Kir7.1 whole-cell currents measured in 5 and 150 mM $[K^+]_o$. In all cases, net currents were <1 nA (−320 and −823 pA, respectively, at −130 mV) at 22°C. The salient features of the expressed Kir7.1 current include weak inward rectification at physiological $[K^+]_o$ and a nonlinear increase of current at negative potentials in both low and high $[K^+]_o$ (Figures 3B, 3C, and 3D). Interestingly, at more depolarized voltages the current inactivates, reducing the current measured at 500 ms to near zero above +50 mV (Figure 3A). Rundown of the whole-cell current was not particularly rapid, with Kir7.1 current declining ~50% over 10 min. Rundown was not affected by inclusion of 4 mM ATP and/or GTP-γ-S in the patch pipette (n = 9). Kir7.1 was highly K^+ selective, as shown by plotting the reversal potential (E_r) as a function of $[K^+]_o$ (Figure 3E). The slope of the E_r versus $[K^+]_o$ relation was 54 mV/decade, close to the 58 mV predicted for a K^+-selective membrane. The nonlinear increase at negative potentials, time-dependent inactivation at positive potentials, slow rundown, and high K^+ selectivity were features of current in all three cell lines expressing Kir7.1. When Kir7.1 was expressed in *Xenopus* oocytes, its current–voltage relation was also nonlinear and the channel was highly K^+ selective (n = 7). Average oocyte Kir7.1 current was ~6 μA at −100 mV (5 mM $[K^+]_o$; data not shown).

A notable feature of Kir7.1 was its low sensitivity to block by external Ba^{2+}, Cs^+, and other potent inward rectifier inhibitory cations. Figure 4 shows the response of Kir7.1 to increasing $[Ba^{2+}]_o$. The EC_{50} for Ba^{2+} block was 1 mM (Figure 4C), independent of the type of cell in which the channel was expressed. Other known inward rectifier K^+ channels are sensitive to inhibition at much

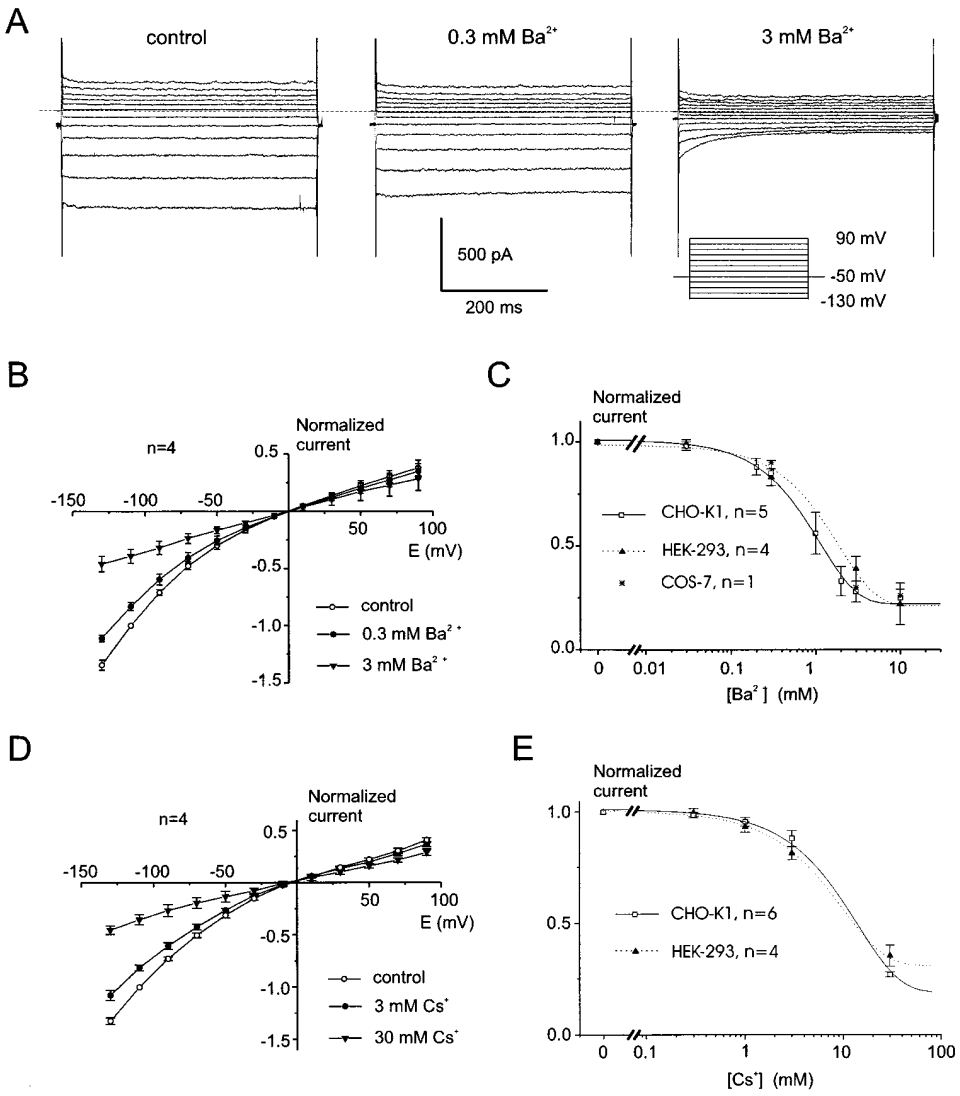

Figure 4. Ba^{2+} and Cs^+ Block Kir7.1

(A) Kir7.1 currents expressed in HEK293 cells. Voltage steps were made from the holding potential (−50 mV) to voltages between −130 mV and 90 mV (ΔV = 20 mV) in control (left) and in the presence of 0.3 (middle) and 3 mM (right) Ba^{2+} as indicated.

(B) Kir7.1 currents measured in HEK293 cells as mean current (400–450 ms of a 500 ms pulse). The current was normalized to the control value at −110 mV and plotted against voltage as indicated (±SEM, n = 4).

(C) Concentration dependence of the Kir7.1 current inhibition by $[Ba^{2+}]_o$ in HEK293 and CHO-K1 cells. Data were fit by a single exponential. The EC_{50} for Ba^{2+} inhibition was between 1 and 2 mM [1.9 mM (HEK293), 1.1 mM (CHO-K1), 1.3 mM (COS7)].

(D) Kir7.1 currents were blocked by external Cs^+. I–V relations measured from HEK293 cells were plotted after block by addition of Cs^+ to the bath (±SEM, n = 4). Currents were normalized to the control value at −110 mV.

(E) Concentration dependence of the Kir7.1 current block by $[Cs^+]_o$ in HEK293, CHO-K1, and COS7 cells. Data were fit using the equation for first-order exponential decay. The EC_{50} was 9.9 ± 0.9 mM for HEK293 and 14.1 ± 1.6 mM for CHO-K1 cells.

lower concentrations (EC_{50}, ~0.1 mM; Kubo et al., 1993a; Bond et al., 1994; Bredt et al., 1995; Takumi et al., 1995, Shuck et al., 1997). Barium block was weakly voltage dependent, in contrast to many other Kir channels (Figure 4B). Similarly, Kir7.1 was not very sensitive to block by external cesium. Figure 4D summarizes the same current–voltage ranges tested in 3 and 30 mM $[Cs^+]_o$. The EC_{50} for Cs^+ block was 10 mM in HEK293 and CHO-K1 cells (Figure 4E). Finally, Kir7.1 was not modulated by even 10 mM external tetraethylammonium chloride (n = 6) and was relatively insensitive to block by 4-aminopyridine (4-AP); 1 mM 4-AP decreased Kir7.1 current by 16% ± 5% and 10 mM 4-AP by 58% ± 4% at −100 mV (n = 4; data not shown).

In an attempt to characterize the single channel properties of Kir7.1, we carried out recordings in cell-attached and excised patch configurations. Under our conditions, no novel single channel activity was observed in CHO-K1, HEK293, or COS7 cells expressing Kir7.1. These experiments were made somewhat difficult by the presence of several channels in native cells, some of which were fairly infrequent and might easily be confused for an expressed current. However, we did not observe single channel currents that were not

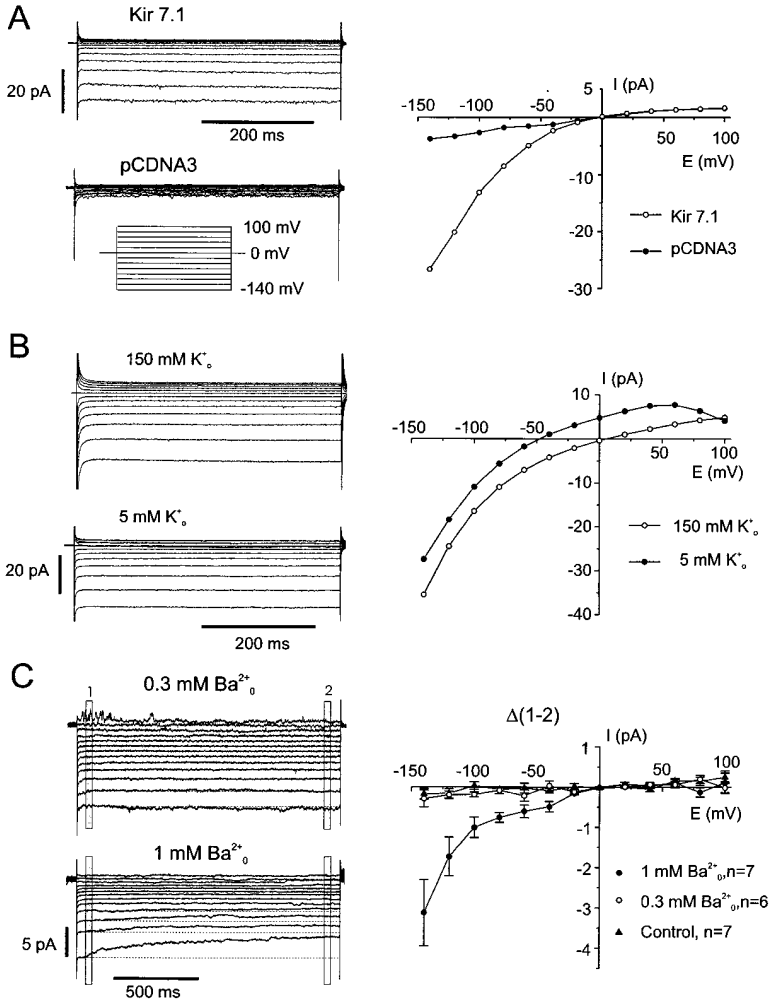

Figure 5. Kir7.1 Patch Current Properties

(A) Traces and I–V plots of cell-attached currents recorded from HEK293 cells transfected with Kir7.1 or pcDNA 3.1, in response to voltage steps from 0 mV to −140 mV and to 100 mV (ΔV = 20 mV). The I–V plot shows mean current measured isochronally between 400 and 450 ms of the 500 ms pulse.

(B) Inside-out currents recorded at different pipette $[K^+]$ (bath $[K^+] = 150$ mM) in response to voltage steps from 0 mV (ΔV = 20 mV). Note that the patch current still rectified at positive potentials despite >4 min washout. In symmetrical $[K^+]$ solution, the slope increased with negative potential. The reversal potential in 5 mM $[K^+]_o$ was −47 ± 5 mV (n = 6), due to leakiness of the patch. Similar results were obtained for 11 CHO-K1 and 8 COS7 cells.

(C) Barium block of cell-attached currents in response to voltage steps from +80 mV (the holding potential was selected to remove Ba^{2+} block). The difference between the mean current amplitudes was measured during periods indicated by the shaded rectangles at the beginning and the end of the voltage pulse (right panel). $[K^+]$ was 150 mM in the bath and pipette. Note that the duration of the voltage pulses was longer than those used for the study of cell-attached currents in the absence of Ba^{2+}, which enhanced resolution of the Ba^{2+} block. No Ba^{2+}-blockable current was observed when the pipette contained 0.3 mM Ba^{2+}.

Note that with 1 mM Ba^{2+} in the pipette, the mean current at the beginning of the negative pulse (11 ± 1 pA, n = 22) was significantly smaller than that measured from the same batch of cells in the absence of Ba^{2+} (27 ± 6 pA, n = 11). Ba^{2+} may have had a fast blocking effect or the channel may have been closed in the presence of Ba^{2+}, as was seen in the whole-cell recording of Figure 3A.

already present in control cells. In ~30% of cell-attached patches in all three expressing cell lines, we observed inwardly directed currents (total, 42 out of 142 patches) similar to those shown in Figure 5A. These currents were never observed in mock-transfected cells (n = 115). The basic properties of the patch current studied in excised patches were indistiguishable from the whole-cell current; the current was highly K^+-selective, inwardly rectifying, and displayed low sensitivity to external Ba^{2+} (Figures 5B and 5C). The current was also characterized by weak rectification at 5 mM $[K^+]_o$ and strong rectification at 150 mM $[K^+]_o$. The rectification persisted even after extensive washout of putative blockers from the inside-out patch (Figure 5B; Lopatin et al., 1994). One striking feature of the current was the very low level of noise around the mean current (Figure 5, see also noise variance in Figure 6B). Such low noise could be explained either by channels with very long open times or by channels of low unitary conductance. Large conductance channels are unlikely to underlie the current because no stepwise decreases in the current decline were observed with 1 mM Ba^{2+} in the pipette after a voltage jump from 80 to −140 mV (Figure 5C, n = 8).

The power spectral density of the current noise displayed a Lorentzian shape, as is typical for ion channels (DeFelice, 1981), and was described by the sum of two Lorentzians (Figure 6A). The fast time constant, reflecting the sum of the channel open and closed times (DeFelice, 1981), was ~1 ms. Nonstationary noise analysis of currents from cell-attached patches recorded at potentials of −100, −120, and −140 mV yielded a single channel conductance of 52 ± 11 fS for HEK293 cells (n = 26; Figure 6B), 55 ± 14 fS for CHO-K1 cells (n = 11), and 43 ± 8 fS for COS7 cells (n = 13). Removal of divalents (2 mM EDTA, no added Mg^{2+} or Ca^{2+}) had no effect on estimated single channel conductance (63 ± 18 fS at −140 mV, n = 11; data not shown).

Other channels known to have very low single channel conductances include the cyclic nucleotide–gated (~100 fS) and calcium release–activated current (CRAC) (~25 fS) channels. Removal of divalent cations dramatically increased the cyclic nucleotide channel (Haynes et al., 1986) and CRAC (Lepple-Wienhues and Cahalan, 1996) conductances. In contrast, Kir7.1's conductance was not noticeably affected by changes in either external or internal divalent cation concentration. Surprisingly, removal of Mg^{2+} from the cytoplasmic side of the patch did not significantly alter the rectification properties of the Kir7.1 channel (n = 4; data not shown). The low single channel conductance and poor sensitivity to cationic

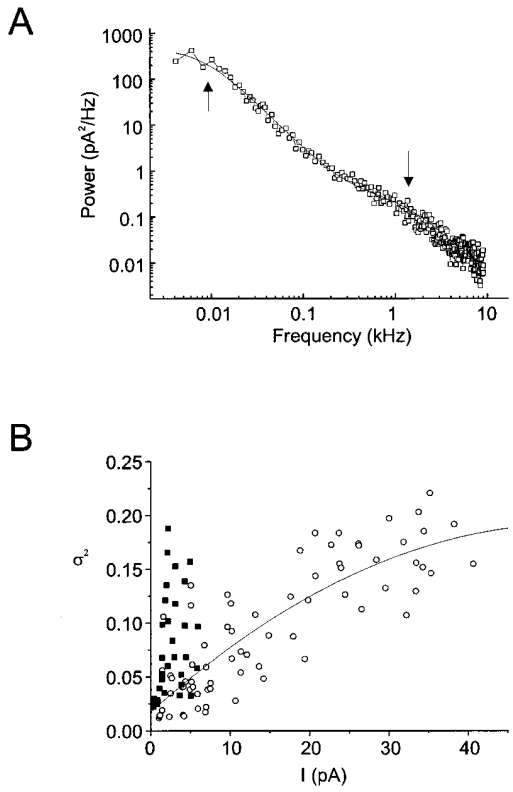

Figure 6. Nonstationary Noise Analysis of Kir7.1 Cell-Attached Currents in HEK293 Cells

(A) Power spectrum of cell-attached currents measured at −140 mV from Kir7.1-transfected cells. The plot represents the subtraction of the mean of eight spectra each for Kir7.1- and mock-transfected cells. The spectra were fit by two Lorentzians calculated as described in the Experimental Procedures (arrows indicate the corner frequencies). The corner frequencies were 1.3 ± 0.17 and 0.008 ± 0.001 kHz (n = 8).

(B) Nonstationary noise analysis of single channel currents in cells expressing Kir7.1 (open circles; n = 26). Mean currents and current variances were determined as described in the Experimental Procedures. From the best fit of the data at −140 mV, the single channel current was estimated to be 0.007 pA (50 fS) with 16,000 Kir7.1 channels/patch. The variance of the current measured from pcDNA 3.1 vector–transfected cells is plotted for comparison (closed rectangles; n = 21).

blockers separated Kir7.1 from all known Kir channels and led us to investigate its unusual pore properties.

Comparison of the amino acid sequence of Kir7.1's pore region with homologous sequences of other cloned Kir channel subunits revealed significant differences in three conserved locations (Figure 7). Ser-111, Met-125, and Gly-129 in Kir7.1 differ from all known Kir family members (more than 100 sequences are represented in the GenBank database). All other Kir family members contained Leu, Arg, and Glu/Asp in these respective positions. Since we obtained and verified the Kir7.1 sequence from several independent libraries, it is unlikely that these changes were due to cloning artifacts. We reasoned that the unusual properties of Kir7.1 might stem from these amino acid substitutions.

To test the hypothesis that these three residues play a role in the unusual pore properties of the Kir7.1 channel, we mutated each of these residues in turn, substituting each with the residues that have been conserved in

Kir 1.1	CVENINGLTSAF**L**FSLETQVTIGYGF**R**CVT**E**ECAT
Kir 1.2	CIMKVDSLTGAF**L**FSLESQTTIGYGV**R**SIT**E**ECPH
Kir 1.3	CVVQVHTLTGAF**L**FSLRSQTTIGYGF**R**YIS**E**ECPL
Kir 2.1	CVSEVNSFTAAF**L**FSIETQTTIGYGF**R**CVT**D**ECPI
Kir 2.2	CVLQVHGFMAAF**L**FSIETQTTIGYGL**R**CVT**E**ECPV
Kir 2.3	CIMHVNGFLGAF**L**FSVETQTTIGYGF**R**CVT**E**ECPL
Kir 3.1	CVANVYNFPSAF**L**FFIETEATIGYGY**R**VIT**D**KCPE
Kir 3.2	CVTNLNGFVSAF**L**FSIETETTIGYGY**R**VIT**D**KCPE
Kir 3.3	CIMHVNGFLGAF**L**FSVETQTTIGYGF**R**CVT**E**ECPL
Kir 3.4	CVENLSGFVSAF**L**FSIETETTIGYGF**R**VIT**E**KCPE
Kir 4.1	CVVQVHTLTGAF**L**FSLESQTTIGYGF**R**YIS**E**ECPL
Kir 5.1	CVDNVHSFTAAF**L**FSLETQTTIGYGY**R**CVT**E**ECSV
Kir 6.1	CVTNVRSFTSAF**L**FSIEVQVTIGFGG**R**MMT**E**ECPL
Kir 6.2	CVTSIHSFSSAF**L**FSIEVQVTIGFGG**R**MVT**E**ECPL
Kir 7.1	CVKYITSFTSAF**S**FSLETQLTIGYGT**M**FPS**G**DCPS

Figure 7. Comparison of Kir Pore Regions

Comparison of the amino acid sequence of the pore region of Kir7.1 with the homologous sequences of cloned inward rectifier K^+ channel subunits. Note that leucine (L), arginine (R), and aspartatic (E) or glutamic acid (D) were conserved in all other inward rectifiers, but are replaced by serine (S), methionine (M), and glycine (G), respectively, in Kir7.1.

the other Kir family members. Western blot analysis and immunostaining of expressing cells with anti-Kir7.1 antibody demonstrated no difference in expression level or plasma membrane localization of mutant proteins compared to the wild-type molecule (data not shown). The whole-cell current measurements demonstrated that mutant channel subunit S111L did not result in any measurable change from native Kir7.1-expressed current (data not shown; n = 27). The mutant channel subunit G129E did not yield measurable currents in either whole-cell or cell-attached recordings (data not shown; n = 65). However, expression of the Kir7.1(M125R) mutant channel subunit produced significantly larger whole-cell currents than wild-type channels. The current was so large that in most cells we were not able to determine the amplitude of this current (measurements were limited by the series resistance of 5–10 MΩ). A 5-fold decrease in the amount of cDNA used for transfection resulted in a decrease in the inward rectifier currents to the 2–4 nA range at −110 mV. The shape of the whole-cell I–V relation was indistinguishable from that of the wild-type channel. The amplitude of Kir7.1(M125R) currents measured in cell-attached patches was at least 30-fold larger than in wild-type Kir7.1-expressing cells (Figure 8A).

Since Western blot and immunocytochemical studies did not reveal any gross changes in channel protein expression or membrane targeting of the M125R mutant, we reasoned that the increase in current expression was due to an increase of either the single channel conductance or mean open time. High resolution recordings of patches expressing Kir7.1(M125R) again did not reveal measurable novel single channel currents, although the noise variance was distinctly higher than that in wild-type Kir7.1-transfected cells (Figure 8B). Power spectral analysis of cell-attached patches held at −80, −100, −120, and −140 mV revealed no changes in channel kinetics of channel opening; the cut-off frequencies of the Lorentzian fits were similar to those observed for the wild-type Kir7.1 channel (1.1 ± 0.12

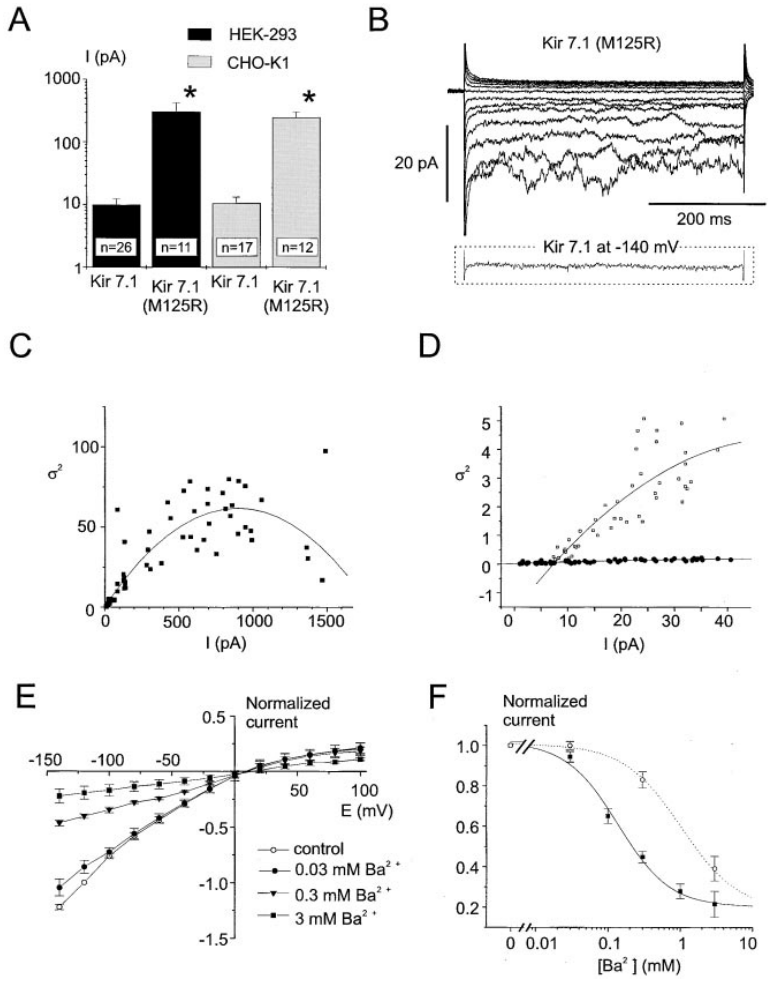

Figure 8. Properties of Mutant Kir7.1(M125R) Channels

(A) Mean Kir7.1(M125R) and Kir7.1 cell-attached currents measured at −120 mV from HEK293 and KIR 7.1 cells, as indicated.

(B, Top) Cell-attached currents in HEK293 cells transfected with Kir7.1(M125R) in response to voltage steps from a holding potential of 0 mV ($\Delta V = 20$ mV).

(B, Bottom) Current at −140 mV reproduced from Figure 4A for comparison. Kir7.1(M125R) expression produced a much larger variance than the Kir7.1 wild-type subunit. In order to compare the noise for Kir7.1(M125R) and Kir7.1, currents of similar amplitude were selected. However, Kir7.1(M125R) currents were 30-fold larger on average (Figure 7A).

(C) Fluctuation analysis of cell-attached currents recorded from cells expressing Kir7.1 (M125R). Mean currents and current variances were determined at −140 mV in 11 cell-attached patches. At −140 mV, the single channel current was ~0.13 pA (930 fS) and N was 12,600.

(D) Expanded plot of variance versus I for currents up to 45 pA (open rectangles). The plot was superimposed upon the plot of variance versus current for Kir7.1 to emphasize the difference in noise properties between the two channel types (Kir7.1 and Kir7.1[M125R]).

(E) Whole-cell currents measured from Kir7.1 (M125R)-transfected HEK293 cells (holding potential = −50 mV; $\Delta V = 20$ mV) in control conditions and in the presence of 0.03, 0.3, and 3 mM Ba^{2+} as indicated (±SEM, n = 4 cells). Currents were normalized to that measured at −110 mV.

(F) Ba^{2+} block of the Kir7.1(M125R) whole-cell current in HEK293 cells. Data were fit by a single exponential decay function (EC_{50} = 0.14 mM). The dotted line and points show data reproduced from Figure 4E for Kir7.1 expressed in HEK293 cells (EC_{50} = 1.1 mM).

and 0.008 ± 0.001 kHz, n = 11, for Kir7.1[M125R] compared to 1.3 ± 0.17 and 0.008 ± 0.001 kHz, n = 8, for wild-type Kir7.1). Nonstationary noise analysis was consistent with a single channel conductance of 930 ± 64 fS, n = 11 (Figures 8C and 8D). Ion selectivity and channel rectification were similar to those of the wild-type channel (data not shown), but sensitivity to Ba^{2+} block was increased by ~10-fold (EC_{50} = 100 μM) to a range that was similar to the Ba^{2+} sensitivity of other Kir channels (Figures 8E and 8F). These properties of the Kir7.1(M125R) mutant suggest that this position is an important determinant of both the single channel conductance and sensitivity to Ba^{2+} blockade.

Discussion

We have cloned a novel member, Kir7.1, of the inward rectifier family of K^+-selective channels. The channel is most homologous (38%) to the ROMK subfamily member Kir1.3 but sufficiently different in both primary structure and function that it should not be assigned to the ROMK family. Kir7.1 has no putative ATP-binding region and no apparent sensitivity to intracellular ATP. The most remarkable features of Kir7.1 relate to its very low single channel conductance (~50 fS) and low sensitivity to blockade by external Ba^{2+}. We attribute these differences to unique residues in the pore domain.

Since the channel is of low conductance and has very little voltage or time dependence in the physiological range, the channel may not have been explicitly identified in previous electrophysiological studies. The channel's distribution in brain, kidney, small intestine, prostate, testis, and other tissues does not suggest any clues to its specific function. However, specific expression of Kir7.1 in neurons but not in glial cells suggests that Kir7.1 has a neuron-specific function. In the absence of any regulatory information, we must assume that the channel simply acts to set the resting membrane potential in the tissues in which it is expressed. The channel is active at rest and undergoes little inactivation. The low conductance of this channel in the setting of a high resistance membrane allows for fine regulation of firing rate. The low noise provided by low conductance background inward rectifier currents should result in fewer firing "errors." Finally, in the absence of other inward rectifier currents, only a few depolarizing channels need

open to overcome a background of many open Kir7.1 channels, thus saving the pump energy required to restore internal cation balance. Another possibility is that the Kir7.1 is just one of the subunits of a native channel. As has been demonstrated for many other channels, additional subunits may contribute significantly to normal function (Isom et al., 1994; Inagaki et al., 1995a; Krapivinsky et al., 1995; Barhanin et al., 1996; McDonald et al., 1997). If so, identification of any putative associating subunits must await purification of native Kir7.1, an avenue that we are currently pursuing.

Heterologously expressed Kir7.1 displays an unusually low single channel conductance and low sensitivity to cationic blockers. We suggested that these unusual properties might be explained by differences in pore structure. Three amino acid residues present in all other Kir pore regions were not conserved in Kir7.1. Replacement of Kir7.1 Met-215 by the respective Kir family-conserved Arg significantly (20- to 30-fold) increased pore conductance and sensitivity to Ba^{2+}. We conclude that this site may play a role in the determination of single channel conductance. The significance of this site for channel conductance and divalent block was recently corroborated by an analagous mutation of the conserved Arg-148 in Kir2.1 (IRK1; Sabirov et al., 1997), which corresponds to the Met-125 position in Kir7.1. Although cells injected with the mutant only expressed detectable current when coexpressed with the wild-type channel subunit, the heteromultimeric single channels were of low conductance. For our channel, we cannot rule out more complicated scenarios, such as the possibility that the substitution results in new heteromultimer formation. If so, the new heteromultimers would have to be present in all three expression systems and would have to account for the identical shape of the I–V relation. At present, we assume the simplest interpretation of our results, that the heterologously expressed channel is a homomultimer of Kir7.1 in both normal and mutant cases. We also substituted two other Kir-conserved amino acids for the corresponding native Kir7.1 residues. The S111L mutation did not change Kir7.1's properties and G129D did not result in functional expression (despite the fact that this Gly was substituted by the conserved Asp found in other Kirs).

Kir7.1 exhibits an unusual current–voltage dependence in that the slope of the I–V relation in both whole-cell and patch currents increases with negative potentials. This increasing nonlinearity was present in both low and high $[K^+]_o$ and in all three cell types expressing Kir7.1. All known inward rectifier channels show a linear current–voltage dependence at negative potentials (Ho et al., 1993; Kubo et al., 1993a, 1993b; Bredt et al., 1995; Inagaki et al., 1995a; Krapivinsky et al., 1995; Takumi et al., 1995). The unusual behavior of Kir7.1 could be explained by the voltage dependence of the channel in the hyperpolarized range. Since the range of voltages below E_K are not usually physiologically relevant, the nonlinearity is more biophysically than functionally important.

One of the interesting features of K^+-selective inward rectifier channels is that their voltage-dependent gating depends on extracellular $[K^+]_o$ and shifts along the voltage axis according to RT $\ln[K^+]_o$. As $[K^+]_o$ increases, so does outward current. The underlying structural mechanism for this behavior is not known, although it has been proposed that it stems from an external K^+-binding site (Ciani et al., 1978). In contrast, as $[K^+]_o$ was increased, Kir7.1's I–V relation did not exhibit the crossover phenomenon (no increase in outward current). The most poorly understood aspect of inward rectifiers relates to the necessary link between the internal Mg^{2+}-binding site and the putative external K^+-binding site (Aleksandrov et al., 1996). Although the M2 putative binding site for Mg^{2+} and polyamines in Kir 7.1 is a negatively charged amino acid (E149), inward rectification is weak. Thus, as for Kir3.2, Kir3.4, Kir1.2, and Kir1.3, Kir7.1 does not obey the proposed correlation between a negatively charged amino acid in this position and strong inward rectification (reviewed by Nichols and Lopatin, 1997). Interestingly, Kir7.1's rectification is also fairly insensitive to removal of internal Mg^{2+}. We can only assume that the unique residues in the channel pore region play a role in the structure of Kir7.1 that change these properties of inward rectification, but complete understanding will require more detailed biophysical study.

In summary, we have cloned a novel inward rectifier K^+ channel with an unusual pore structure, which results in a low single channel conductance, low sensitivity to common external K^+ channel blockers, and unique dependence of rectification on $[K^+]_o$. The channel is expressed in a wide array of tissues, including brain, where it is specifically located in neurons. The channel does not appear to be regulated and may be responsible for setting resting membrane potentials in a diverse array of tissues.

Experimental Procedures

Cloning of Kir7.1

EST clone *260707* was sequenced in both directions and a 800 bp fragment containing the putative coding region was used for library screening. About 10^6 clones from the human fetal brain λ cDNA library (Uni-Zap XR, Stratagene) were screened with the probe labeled with [α-^{32}P]dCTP (DuPont NEN) by random priming (Prime-It-II, Stratagene). Hybridization was performed in 2× PIPES buffer (0.8 M NaCl, 0.02 M PIPES buffer [pH 6.5]), 50% deionized formamide, 0.5% SDS, and 100 μg/ml denatured salmon sperm DNA at 42°C for 16 hr. The membranes were subsequently washed four times with 0.1× SSC, 0.1% SDS for 20 min each at temperatures from 55°C–65°C. Phages found to hybridize to the probe were plaque purified and excised as a pBluescript SK phagemid (Stratagene), and both strands were sequenced using automated dideoxy terminator sequencing on a 377 ABI DNA Sequencer (Applied Biosystems).

Site-directed mutagenesis was accomplished by megaprimer PCR with Pfu polymerase (Stratagene). The megaprimers were amplified using a mutant sense primer (Ser-111 to Leu: 5′-GTTTCACAG CTGCATTCCTCTTCTCCCTGGAGACAC-3′; Met-125 to Arg: 5′-CAA TTGGTTATGGTACCCGGTTCCCCAGTGGTGACT-3′; Gly-129 to Glu: 5′-ACCATGTTCCCCAGTGAGGACTGTCCAAGTGCAATC-3′) and a vector antisense primer containing a XhoI site (5′-GCAAACAACAGA TGGCTGGCAACTAGAAGGCACAGTCGAG-3′) from a pcDNA/Kir7.1 template. For PCR, initial denaturation at 95°C for 3 min was followed by 10 cycles at 95°C for 30 s, 65°C for 30 s, and 72°C for 3 min with a final extension step at 72°C for 10 min. The megaprimer was purified and used in a second PCR reaction with a vector sense primer containing a BamHI site (5′-TACGACTCACTATAGGGAGA CCCAAGCTGGCTAGCGTTA-3′) to produce the full-length mutant Kir7.1. The PCR fragment was then subcloned back into the BamHI and XhoI sites of pcDNA 3.1, and the mutations were confirmed by

sequencing both strands of the insert. Nucleotide and amino acid sequences were analyzed with GeneWorks (IntelliGenetics) and MacVector (Oxford Molecular Group) programs.

Analysis of Gene Expression

Human multiple tissue cDNA (MTC; Clontech) panels were PCR screened with primers flanking bases 372–1023 of the Kir7.1 coding sequence. A fragment of the expected size, 650 bp, was PCR amplified from certain tissues. A multitissue human Northern blot (Clontech) was probed with a [^{32}P]dCTP random-labeled fragment (Stratagene) containing bases 318–1023 of the Kir7.1 coding sequence.

Immunochemistry

A rabbit anti-IBP72 antibody was generated against the GST–Kir7.1 (amino acids 284–351) fusion protein and affinity-purified on immobilized GST–Kir7.1 from anti-GST–depleted sera. This purified antibody specifically recognized a 45 kDa band in Kir7.1-transfected but not in mock-transfected cells. For immunoblotting, SDS-PAGE–separated proteins were electrotransferred to polyvinylidene difluoride (PVDF) membrane (Millipore), probed with anti-Kir7.1 and anti-rabbit peroxidase (Pierce), and visualized with enhanced chemiluminescence (ECL) (Amersham). For immunocytochemistry, HEK293 cells were grown to 20% confluency on coverslips and then transfected with Kir7.1 and the green fluorescent protein (GFP) DNA. After visible GFP expression, cells were fixed in solution containing 3% paraformaldehyde and permeabilized with 0.1% Triton X-100. Cells were blocked with 3% BSA for 1 hr and then incubated with anti-Kir7.1 (5 μg/ml) followed by rhodamine-conjugated anti-rabbit (Cappel) IgG secondary antibodies. Primary cultures of hippocampal neurons were prepared from 2-day-old neonatal rats as described (Medina et al., 1996). The cultured cells were used for immunofluorescence analysis 20 days after development in vitro. In controls, the anti-Kir7.1 antibody was blocked with antigen fusion protein (0.6 μM). Anti-β-tubulin III monoclonal antibody (Sigma) was visualized using anti-mouse fluorescein conjugate (Pierce). Immunofluorescent images were obtained by confocal microscopy (Zeiss LSM 410). Rat brain slices (50 μm thick) were prepared from adult rats as described earlier (Drake et al., 1997) and immunochemically labeled with aKir7.1 antibody using an immunoperoxidase labeling kit (Pierce) according to the manufacturer's protocol.

Heterologous Expression and Electrophysiological Analysis

CHO-K1, HEK293, and COS7 cells were cultured as recommended by the American Type Culture Collection (ATCC). Cells were plated at 10^6 cells/100 mm dish 1 day prior to transfection. Cells were transfected using the standard Ca^{2+} phosphate method (Sambrook et al., 1989). Each 100 mm plate was transfected with 15 μg of plasmid (pcDNA 3.1, Invitrogen) DNA containing either wild-type or mutant Kir7.1 cDNA and 3 μg pGreen Lantern–GFP (Gibco BRL). GFP expression in transfected cells was visualized with an inverted fluorescence microscope. All cells expressing GFP also expressed Kir7.1, as demonstrated by immunofluorescent staining with anti-Kir7.1 antibody.

Electrophysiological recordings were performed from isolated cells using the patch-clamp technique in whole-cell, cell-attached, or inside-out configurations. Currents were recorded using an Axopatch 200B amplifier (Axon Instruments). Data were filtered at 5 kHz, digitized at 20 kHz through a 1200 DigiData A–D converter using pClamp6 software (Axon Instruments) and stored on disk for offline analysis. Unless otherwise mentioned in the text, the internal pipette solution contained (in mM): KCl 140, EGTA 1.1, $CaCl_2$ 0.06, HEPES-K 10, and $MgCl_2$ 2.0 (pH 7.2). The resistance of the recording borosilicate glass pipettes was 2–4 MΩ, and series resistance was in the range of 10–30 MΩ. The 150 mM $[K^+]_o$ external solution used for whole-cell and cell-attached recordings contained (in mM): KCl 140, $CaCl_2$ 0.1, $MgCl_2$ 2.0, and HEPES-K 10 (pH 7.4). To study the selectivity of the channel, K^+ was substituted by Na^+ as indicated in the text. Before excision of inside-out patches, the bath solution was replaced with internal solution.

Nonstationary noise analysis (Sigworth, 1977; Sigworth and Zhou, 1992) was carried out on cell-attached currents (f_0 = 5 kHz, sample rate = 20 kHz) displaying time-dependent decay of the mean current by 30%–60% at constant voltage (−80, −100, −120, and −140 mV in symmetrical 150 mM $[K^+]$). In some experiments, 1 mM Ba^{2+} (Kir7.1) or 0.1 mM Ba^{2+} (Kir7.1[M125R]) was included in the pipette solution to induce current inactivation as described in the text (Makhina et al., 1994). Mean current (I) and variance (σ^2) were calculated using pClamp6 software from four to eight 200 ms segments recorded at the different times and showing different mean current values. The single channel current (i) was determined for each experiment by fitting the equation $\sigma^2 = iI - I^2/N + B$, using a least-squares algorithm, where σ^2 was the variance, I was the mean cell-attached current, N was the number of active channels, and B was a free parameter reflecting the background noise. Parabolas shown in Figures 6B and 8C are the best fit to all data obtained for HEK293 cells using the above equation.

Power-density spectra were calculated using a fast Fourier transform provided by Origin Software (Microcal) from 2 s segments of cell-attached records. The data were fit by a nonlinear least-squares algorithm to the following equation (DeFelice, 1981): $S(f) = (S_0)'f_c'^2/([f_c']^2 + f^2) + (S_0)''f_c''^2/([f_c'']^2 + f^2)$, where S_0 is the power density, S(f) is the spectral current density at a given frequency f, and f_c is the corner frequency. All data are presented as mean ± SEM.

Acknowledgments

This work was supported by the National Institutes of Health (NHLBI 54873 to D. E. C.; NIH NIDDK 09432 to Y. Y.) and by the Howard Hughes Medical Institute. We are grateful to Dr. Andrei Aleksandrov for helpful discussion and critical reading of the manuscript and Rern Lau for excellent technical support.

Received January 27, 1998; revised April 10, 1998.

References

Aleksandrov, A., Velimirovic, B., and Clapham, D.E. (1996). Inward rectification of the IRK1 K^+ channel reconstituted in lipid bilayers. Biophys. J. *70*, 2680–2687.

Barhanin, J., Lesage, F., Guillemare, E., Fink, M., Lazdunski, M., and Romey, G. (1996). K(V)Lqt1 and Isk (Mink) proteins associate to form the I-Ks cardiac potassium current. Nature *384*, 78–80.

Bond, C.T., Pessia, M., Xia, X.M., Lagrutta, A., Kavanaugh, M.P., and Adelman, J.P. (1994). Cloning and expression of a family of inward rectifier potassium channels. Receptors Channels *2*, 183–191.

Bredt, D.S., Wang, T.L., Cohen, N.A., Guggino, W.B., and Snyder, S.H. (1995). Cloning and expression of two brain-specific inward rectifier potassium channels. Proc. Natl. Acad. Sci. USA *92*, 6753–6757.

Ciani, S., Krasne, S., Miyazaki, S., and Hagiwara, S. (1978). A model for anomalous rectification: electrochemical-potential–dependent gating of membrane channels. J. Membr. Biol. *44*, 103–34.

DeFelice, L.J. (1981). Introduction to Membrane Noise (New York: Plenum Press), pp. 115–332.

Doyle, D.A., Joao, M.C., Pfuetzner, R.A., Kuo, A., Gulbis, J.M., Cohen, S.L., Chait, B.T., and MacKinnon, R. (1998). The structure of the potassium channel: molecular basis of K^+ conduction and selectivity. Science *280*, 69–76.

Drake, C.T., Bausch, S.B., Milner, T.A., and Chavkin, C. (1997). Girk1 immunoreactivity is present predominantly in dendrites, dendritic spines, and somata in the CA1 region of the hippocampus. Proc. Natl. Acad. Sci. USA *94*, 1007–1012.

Hagiwara, S., Miyazaki, S., and Rosenthal, N.P. (1976). Potassium current and the effect of cesium on this current during anomalous rectification of the egg cell membrane of a starfish. J. Gen. Physiol. *67*, 621–638.

Haynes, L.W., Kay, A.R., and Yau, K.W. (1986). Single cyclic GMP–activated channel activity in excised patches of rod outer segment membrane. Nature *321*, 66–70.

Ho, K., Nichols, C.G., Lederer, W.J., Lytton, J., Vassilev, P.M., Kanasirska, M.V., and Hebert, S.C. (1993). Cloning and expression of an inward rectifier ATP-regulated potassium channel. Nature *362*, 31–37.

Inagaki, N., Gonoi, T., Clement, J.P., Namba, N., Inazawa, J., Gonzalez, G., Aguilarbryan, L., Seino, S., and Bryan, J. (1995a). Reconstitution of IKATP—an inward rectifier subunit plus the sulfonylurea receptor. Science *270*, 1166–1170.

Inagaki, N., Tsuura, Y., Namba, N., Masuda, K., Gonoi, T., Horie, M., Seino, Y., Mizuta, M., and Seino, S. (1995b). Cloning and functional characterization of a novel ATP-sensitive potassium channel ubiquitously expressed in rat tissues, including pancreatic islets, pituitary, skeletal muscle, and heart. J. Biol. Chem. *270*, 5691–5694.

Isom, L.L., De Jongh, K.S., and Catterall, W.A. (1994). Auxiliary subunits of voltage-gated ion channels. Neuron *12*, 1183–1194.

Krapivinsky, G., Gordon, E., Wickman, K., Velimirovic, B., Krapivinsky, L., and Clapham, D.E. (1995). The G protein–gated atrial K^+ channel, I_{KACh}, is a heteromultimer of two inward rectifier K^+ channel proteins. Nature *374*, 135–141.

Kubo, Y., Baldwin, T.J., Jan, Y.N., and Jan, L.Y. (1993a). Primary structure and functional expression of a mouse inward rectifier potassium channel. Nature *362*, 127–132.

Kubo, Y., Reuveny, E., Slesinger, P.A., Jan, Y.N., and Jan, L.Y. (1993b). Primary structure and functional expression of a rat G protein–coupled muscarinic potassium channel. Nature *364*, 802–806.

Lepple-Wienhues, A., and Cahalan, M.D. (1996). Conductance and permeation of monovalent cations through depletion-activated Ca^{2+} channels (I_{CRAC}) in Jurkat T cells. Biophys. J. *71*, 787–794.

Lopatin, A.N., Makhina, E.N., and Nichols, C.G. (1994). Potassium channel block by cytoplasmic polyamines as the mechanism of intrinsic rectification. Nature *372*, 366–369.

Makhina, E.N., Kelly, A.J., Lopatin, A.N., Mercer, R.W., and Nichols, C.G. (1994). Cloning and expression of a novel human brain inward rectifier potassium channel. J. Biol. Chem. *269*, 20468–20474.

McDonald, T.V., Yu, Z.H., Ming, Z., Palma, E., Meyers, M.B., Wang, K.W., Goldstein, S.A.N., and Fishman, G.I. (1997). A MinK-HERG complex regulates the cardiac potassium current IKr. Nature *388*, 289–292.

Medina, I., Filippova, N., Bakhramov, A., and Bregestovski, P. (1996). Calcium-induced inactivation of NMDA receptor channels evolves independently of run-down in cultured rat brain neurones. J. Physiol. *495*, 411–427.

Nichols, C.G., and Lopatin, A.N. (1997). Inward rectifier potassium channels. Annu. Rev. Physiol. *59*, 171–191.

Sabirov, R.Z., Tominaga, T., Miwa, A., Okada, Y., and Oiki, S. (1997). A conserved arginine residue in the pore region of an inward rectifier K^+ channel (IRK1) as an external barrier for cationic blockers. J. Gen. Physiol. *110*, 665–677.

Sambrook, J., Fritsch, E.F., and Maniatis, T. (1989). Molecular Cloning: A Laboratory Manual, Second Edition, Volume 3 (Cold Spring Harbor, NY: Cold Spring Harbor Laboratory Press).

Shuck, M.E., Piser, T.M., Bock, J.H., Slightom, J.L., Lee, K.S., and Bienkowski, M.J. (1997). Cloning and characterization of two K^+ inward rectifier (Kir) 1.1 potassium channel homologs from human kidney (Kir1.2 and Kir1.3). J. Biol. Chem. *272*, 586–593.

Sigworth, F.J. (1977). Sodium channels in nerve apparently have two conductance states. Nature *270*, 265–267.

Sigworth, F.J., and Zhou, J. (1992). Ion channels. Analysis of nonstationary single-channel currents. Methods Enzymol. *207*, 746–762.

Takumi, T., Ishii, T., Horio, Y., Morishige, K.I., Takahashi, N., Yamada, M., Yamashita, T., Kiyama, H., Sohmiya, K., Nakanishi, S., and Kurachi, Y. (1995). A novel ATP-dependent inward rectifier potassium channel expressed predominantly in glial cells. J. Biol. Chem. *270*, 16339–16346.

Walker, J.E., Saraste, M.J., Runswick, M.J., and Gay, N.J. (1982). Distantly related sequences in the alpha and beta subunits of ATP synthetase, myosin, kinases, and other ATP-requiring enzymes and a common nucleotide binding fold. EMBO J. *1*, 945–951.

GenBank Accession Number

The nucleotide sequence of the novel Kir7.1 channel has been submitted to GenBank under accession number AF061118.